UC Davis
UC Davis Previously Published Works

Title
Dopant Concentration Controls Quasi-Static Electrostrictive Strain Response of Ceria Ceramics

Permalink
https://escholarship.org/uc/item/2p27705m

Journal
ACS Applied Materials & Interfaces, 12(35)

ISSN
1944-8244

Authors
Varenik, Maxim
Nino, Juan Claudio
Wachtel, Ellen
et al.

Publication Date
2020-09-02

DOI
10.1021/acsami.0c07799

Peer reviewed

ACS APPLIED MATERIALS & INTERFACES

Research Article

Dopant Concentration Controls Quasi-Static Electrostrictive Strain Response of Ceria Ceramics

Maxim Varenik, Juan Claudio Nino, Ellen Wachtel, Sangtae Kim, Ori Yeheskel, Nimrod Yavo, and Igor Lubomirsky*

Cite This: *ACS Appl. Mater. Interfaces* 2020, 12, 39381−39387

Read Online

ACCESS | Metrics & More | Article Recommendations | Supporting Information

ABSTRACT: Electromechanically active ceramic materials, piezoelectrics and electrostrictors, provide the backbone of a variety of consumer technologies. Gd- and Sm-doped ceria are ion conducting ceramics, finding application in fuel cells, oxygen sensors, and, potentially, as memristor materials. While optimal design of ceria-based devices requires a thorough understanding of their mechanical and electromechanical properties, reports of systematic study of the effect of dopant concentration on the electromechanical behavior of ceria-based ceramics are lacking. Here we report the longitudinal electrostriction strain coefficient (M_{33}) of dense $RE_xCe_{1-x}O_{2-x/2}$ ($x \leq 0.25$) ceramic pellets, where RE = Gd or Sm, measured under ambient conditions as a function of dopant concentration within the frequency range $f = 0.15-350$ Hz and electric field amplitude $E \leq 0.5$ MV/m. For >100 Hz, all ceramic pellets tested, independent of dopant concentration, exhibit longitudinal electrostriction strain coefficient with magnitude on the order of 10^{-18} m²/V². The quasi-static ($f < 1$ Hz) electrostriction strain coefficient for undoped ceria is comparable in magnitude, while introducing 5 mol % Gd or 5 mol % Sm produces an increase in M_{33} by up to 2 orders of magnitude. For $x \leq 0.1$ (Gd)−0.15 (Sm), the Debye-type relaxation time constant (τ) is in the range 60−300 ms. The inverse relationship between dopant concentration and quasi-static electrostrictive strain parallels the anelasticity and ionic conductivity of Gd- and Sm-doped ceria ceramics, indicating that electrostriction is partially governed by ordering of vacancies and changes in local symmetry.

KEYWORDS: electrostriction, anelasticity, doped ceria, point defects, elastic moduli, ultrasonic time of flight, nanoindentation, primary creep
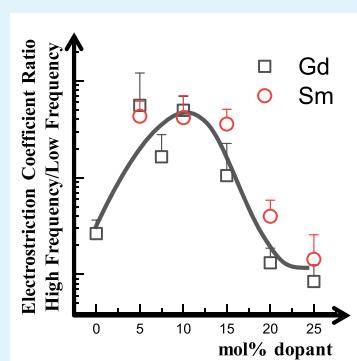
1. INTRODUCTION

Gd- and Sm-doped ceria are among the most extensively studied examples of solid-state ionic conductors,[1] finding application in fuel cells, sensors,[2] and, potentially, as memristor materials.[3] Optimal engineering design of ceria-based devices requires understanding their mechanical and electromechanical properties, which have recently been shown to be unexpectedly complex. Gd-doped ceria (GdDC, a.k.a. cerium gadolinium oxide, CGO) ceramics and thin films, although equilibrium solids, exhibit time-dependent elastic moduli; that is, they are anelastic under anisotropic applied stress.[4−7] Gd- and Sm-doped ceria (SmDC, a.k.a. cerium samarium oxide, CSO) ceramics and thin films exhibit room temperature, recoverable, mechanical creep under nanoindenter load hold.[8−10] The dependence of Poisson's ratio on strain magnitude,[11,12] spontaneous volume expansion over time, and hysteresis of the cubic lattice parameter during thermal cycling[5,13] have also been reported. These mechanical anomalies have tentatively been ascribed to symmetry-lowering lattice distortions, that is, elastic dipoles created in the vicinity of charge-compensating oxygen vacancies, which, depending on the dopant concentration, can occupy a few percent of the anion sublattice sites.[14−17] We have recently shown[9] that the dominant

anelastic behavior of Sm-doped ceria ceramics decreases with dopant concentration ($x = 0.05−0.25$). From these data, we concluded that the transition at $x \approx 0.25−0.3$ from the fluorite ($Fm\overline{3}m$) phase to the double-fluorite ($Ia\overline{3}$) phase, with attendant oxygen vacancy ordering, can restore predominantly elastic behavior.

Although mechanical properties of Sm- and Gd-doped ceria ceramics have been reported, how the electromechanical behavior, in particular, nonclassical electrostriction, observed to date in Gd-doped ceria,[14,18−21] (Y,Nb)-stabilized δ-Bi₂O₃,[22] and La₂Mo₂O₉[23] depends on dopant concentration has not been systematically studied. Previously published data[21,24,25] from 10 mol % Gd-doped ceria (10GdDC) ceramics exhibit strain saturation in strong electric fields and frequency relaxation with a characteristic relaxation time of a fraction of a second. A deeper understanding of the phenomenon of
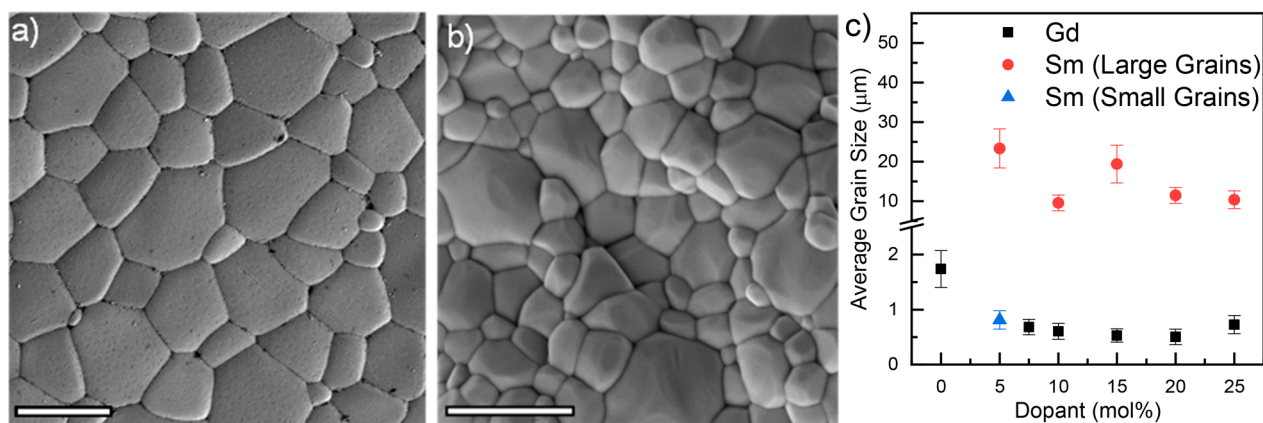
Figure 1. (a) SEM images of the polished surfaces of (a) 10 mol % Sm-doped and (b) 7.5 mol % Gd-doped ceria ceramic pellets; scale bars: 10 and 1 μm, respectively. (c) Number-average grain size measured on SEM images by using the lineal intercept method, including ×1.56 correction to account for grains that may be only partially visible at the image surface.[29] Error bars are standard deviation for ≥100 grains.

electrostriction in aliovalent doped ceria ceramics requires systematic investigation of the concentration dependence of the electrostriction properties in phases with randomly distributed oxygen vacancies as well as those where the onset of ordering can be detected. Here we report results of a systematic study of the longitudinal electrostriction strain coefficient M_{33} of dense $RE_xCe_{1-x}O_{2-x/2}$ ($x \leq 0.25$) ceramics, where $RE = Gd^{3+}$ or Sm^{3+}, as a function of dopant concentration within the frequency range 0.15−350 Hz and electric field amplitude 0−0.5 MV/m.

2. EXPERIMENTAL SECTION

2.1. Ceramic Preparation. Samples of SmDC, $Sm_xCe_{1-x}O_{2-x/2}$ ($0.05 \leq x \leq 0.25$), were synthesized via conventional solid-state reactions and procedures as previously described.[26,27] Briefly, Sm_2O_3 and CeO_2 powders (both 99.99% purity, Alpha Aesar) were ball-milled, dried, and calcined at 1450 °C for 10 h. Up to 2 wt % binder (PVA dissolved in deionized water) was added to the powders, and cylindrical pellets were formed in metal dies by uniaxial pressing. It is important to note that the presence of PVA does not modify mechanical properties, particularly since the green ceramics undergo sintering.[9] The pellets were then subjected to isostatic pressing at 250 MPa for 3 min. The pellets were sintered at 1600 °C for 10 h ($x \leq 0.25$) or 1690 °C for 5 h ($0.30 \leq x \leq 0.35$).

$Gd_xCe_{1-x}O_{2-x/2}$ ($0 \leq x \leq 0.25$) powders were synthesized by a coprecipitation method.[28] A 0.7 M aqueous solution of $(NH_4)_2CO_3$ (99% extra pure, Arcos Organics) was added dropwise to an aqueous solution containing the amounts of $Gd(NO_3)_3 \cdot 6H_2O$ and $Ce(NO_3)_3 \cdot 6H_2O$ (0.3 M, total solute, purity 99.9%, Strem) required to provide the Gd concentrations desired. This mixture was kept at 80 °C under continuous stirring for 1 h. The precipitates were then collected by centrifugation, washed three times with water and then with ethanol, and afterward allowed to dry at 120 °C for 12 h. The resulting powders were ground, sifted through a 50 μm mesh, and calcined in air at 495 °C for 2 h. Cylindrical pellets were then formed by cold isostatic pressing of the powders at 300 MPa, followed by rapid sintering, with optimal temperatures and times as reported in refs 21 and 28.

2.2. Ceramic Pellet Characterization. X-ray diffraction profiles have been reported previously[9,28] and demonstrate that all pellets are in the fluorite phase, with only a weak admixture of the double fluorite phase in the 27 mol % Gd-doped sample.[26]

The number-average grain size of the SmDC pellets was determined by the lineal intercept method[29] on SEM images (Zeiss Sigma 500) to be ≥10 μm,[9] without obvious dependence on Sm concentration (Figure 1a−c).

The number-average grain size of the Gd-doped ceramic pellets was determined by SEM to be ∼0.5 μm for the doped samples and ∼1.5 μm for undoped CeO_2 (Figure 1b,c) and is weakly dependent on doping level. One 5 mol % Sm-doped ceria pellet was also prepared according to the coprecipitation protocol. The number-average grain size was ∼0.7 μm according to SEM. EDAX (Bruker XFlash/60) was used to estimate dopant concentration; the uncertainty in the reported concentration is ±1 mol %. The pellet density was measured by the conventional Archimedes method (Figure 2).[28] At 25 mol %
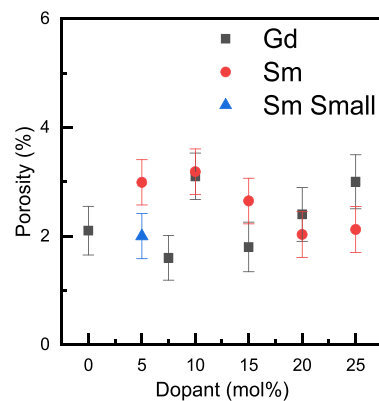
Figure 2. Ceramic pellet porosity, $(1 - \text{density}_{measured}/\text{density}_{theoretical})$, determined by the Archimedes flotation method, described in ref 28 as a function of dopant concentration. A single 5 mol % Sm-doped ceria pellet (Sm small) was prepared according to the protocol described for GdDC pellets. Error bars are calculated on the basis of statistical uncertainty from five measurements.

doping and below, the porosity ($1 - \text{density}_{measured}/\text{density}_{theoretical}$) of both Sm- and Gd-doped pellets was <4%. Sample pellets were polished; top and bottom faces were made parallel with silicon carbide polishing papers (up to 1600 mesh) and then washed with 100% ethanol in an ultrasonic bath for 30 min to remove silicon carbide residue. All samples were reoxidized, prior to electromechanical measurements, at 500 °C for 5 h in a pure oxygen atmosphere. Pellet dimensions were 6−8 mm in diameter and ∼1 mm thickness.

2.3. Electrostrictive Strain Measurements. Longitudinal (i.e., parallel to the applied electric field) electrostrictive strain, u_{33}, was measured with instrumentation described previously.[21,22] Briefly, the ceramic pellet was inserted between two electrodes, the top electrode being spring-loaded (Figure 3).

A pushrod was used to transfer displacement from the electrodes to a proximity sensor (Capacitance, CPL190 Lion); the signal from the proximity sensor was read with a lock-in amplifier (DSP 7265).

Figure 3. Diagram of the equipment used to measure electrostrictive strain, including the top spring-loaded aluminum electrode, the doped ceria pellet, and thin film contacts (when applicable; see Figure S1).

Longitudinal electrostrictive strain is calculated as the ratio between the displacement and the original thickness of the ceramic pellets as measured with a micrometer screw gauge (Mitutoyo 193-111, ±2 μm). Measurements were performed under ambient conditions (24 ± 2 °C, relative humidity 20%−55%). Commercial samples of PMN-PT with silver metal contacts (TRS Technologies; our measurement M_{33} = (3.5 ± 0.5) × 10^{-16} m^2/V^2) and a piezoelectric 100-cut quartz single crystal without additional sputtered metal contacts (our measurement, longitudinal piezoelectric coefficient d_{33} = 2.3 ± 0.2 pm/V) were used to calibrate the proximity sensor/lockin-in amplifier pair. For these samples, no dependence on frequency (150 mHz− 1000 Hz) could be detected.

Mirror-polished aluminum plates were used as the electrodes for these measurements. Metallic contacts that block ion transport (e.g., Ni, Cr, Ag, and Au) have been shown to suppress electrostriction in ceria-based thin films due to the formation of blocking layers,[18,19,30,31] which presumably develop as a result of ion migration and space-charge formation. When metals support oxygen ion exchange with aliovalent cation-doped ceria thin films, then the electro-chemo-mechanical effect (material expansion due to electric-field-induced oxygen diffusion) becomes dominant at low frequencies.[30] Therefore, in earlier work,[21] aluminum electrodes were generally used. In the present report, we have also tested the effects of the addition of sputtered TiN films, as conductive but nonmetallic contacts, as well as sputtered Ta$_2$O$_5$(20 nm)/Ta films. Although TiN and Ta$_2$O$_5$(20 nm)/Ta are apparently superior to metallic contacts, they are nevertheless inferior to bare Al electrodes (Figure S1) at frequencies below 10 Hz, where the influence of contact chemistry is strong.

3. RESULTS AND DISCUSSION

3.1. Longitudinal Electrostrictive Strain. Unlike piezo-electric materials, all dielectric solids, irrespective of symmetry, can display electrostrictive behavior in an externally applied electric field. In the case of electrostrictors, the induced longitudinal strain (u_{33}) is linearly proportional to the square of the amplitude of the applied field (E^2) and is detected at the second harmonic of the field frequency:

$$u_{33} = E_z{}^2 M_{33} \qquad (1)$$

Because of the work of Newnham et al.,[32,33] we also know that the magnitude of the electrostrictive response of materials as

diverse as inorganic oxides and relaxor ferroelectrics generally scales with the ratio of the elastic compliance (inverse Young's modulus) to the dielectric constant. As such, doped ceria ceramics with elastic moduli in the GPa range would not appear to be promising candidates for displaying large electrostrictive strain. However, quadratic electromechanical coupling is also commonly attributed to the anharmonic form of interatomic potentials, for which strong evidence has been found for ceria solid solutions.[16,34] Indeed, dense ceramic pellets RE$_x$Ce$_{1-x}$O$_{2-x/2}$ ($x \leq 0.25$), where RE = Gd^{3+} or Sm^{3+}, all display room temperature electromechanical coupling at the second harmonic of the applied AC electric field. Induced longitudinal strain exceeds that predicted on the basis of the classical (Newnham) scaling law by up to 3 orders of magnitude (Figures 4 and 5; also see section 2 in the

Figure 4. (a) Longitudinal electrostrictive strain ($|u_{33}|$) measured for 15 mol % samarium-doped ceria ceramic pellets as a function of the square of the electric field E. Nonlinear dependence is observed for low frequency ($f \sim 0.15-1.3$ Hz) measurements for $E^2 \leq 0.05$ MV^2/m^2; higher frequency measurements ($f > 10$ Hz) display linear dependence over the complete range of electric fields examined. Solid lines are fits to eq 1, and dashed lines are extrapolated from the low field region. (b) When doping is increased to 25 mol % Sm, the strain magnitude is significantly reduced while the linear dependence is observed at all frequencies over the complete range of electric fields examined. Measurements were made in triplicate. Error bars include both statistical uncertainty and instrumental accuracy.

Supporting Information). Interestingly, Sm- and Gd-doped pellets contract in the direction of the applied field; thus, both strain and longitudinal electrostriction coefficients, M_{33}, are negative (for simplicity, $|u_{33}|$ and $|M_{33}|$ values are presented). The fact that ceria solid solution ceramics contract in an

Figure 5. Electrostrictive longitudinal strain $|u_{33}|$ in (a) 10 mol % and (b) 25 mol % GdDC ceramics measured as described in the caption to Figure 4. Error bars are based on measurement statistical uncertainty and instrumental accuracy.

electric field excludes the possibility that the observed effect is related to thermal expansion or to expansion derived from chemical reduction.[35] Other materials with $M_{33} < 0$ include fluorides that crystallize in the same space group as ceria ($Fm\overline{3}m$), such as CaF_2;[32] however, most electrostrictive oxides expand in an electric field[32] (see sections 2 and 3 in the Supporting Information). For undoped ceria and for $RE_xCe_{1-x}O_{2-x/2}$ ($x \leq 0.25$) samples with $x > 0.15$ (RE = Sm^{3+}) or $x > 0.1$ (RE = Gd^{3+}), the longitudinal strain $|u_{33}|$ is linearly related to the square of the electric field (Figures 4b and 5b) over the complete range tested ($E \leq 0.5$ MV/m; $f = 0.15-350$ Hz).

This, in addition to the second harmonic response, clearly identifies the dimensional change as being due to electrostriction. However, for more lightly doped samples with $x \leq 0.15$ (Sm) or $x \leq 0.1$ (Gd), the observable electrostrictive strain deviates from linear behavior in strong, quasi-static ($f < 2$ Hz) electric fields (Figures 4a and 5a) where the onset of nonlinearity was determined to be 0.1−0.2 MV/m. Because nonlinearity is observed only at low frequencies and high field, we suggest that under these conditions elastic dipoles begin to fully align with the electric field. At full alignment, no additional strain can be produced. This behavior is similar to that observed by[21] in which the onset of nonlinearity for 10 mol % GdDC ceramic pellets was found to be approximately at field strength 0.17 MV/m. The electrostriction strain coefficients derived for quasi-static measurements on lightly doped samples are calculated by linear fitting (eq 1) below 0.2 MV/m.

3.2. Frequency Relaxation. The electrostrictive strain coefficient $|M_{33}|$ for samples with dopant concentration ≤ 15 mol % Sm or ≤ 10 mol % Gd exhibits marked Debye-type relaxation with increasing E-field frequency f (Figure 6a,c). The Debye relaxation of the electrostrictive strain coefficient as a function of frequency is described by the equation

$$M_{33} = M_{33}^0 / \sqrt{(2\pi f \tau)^2 + 1} + M_{33}^\infty \qquad (2)$$

where M_{33}^∞ and M_{33}^0 are the electrostriction coefficients at $f \rightarrow \infty$ and $f \rightarrow 0$, respectively and τ is a characteristic relaxation time (Table 1).

The Levenberg−Marquardt algorithm fitting finds values of τ that range between 60 and 300 ms and low-field/low-frequency electrostriction strain coefficients $|M_{33}^0| \approx 10^{-17}-10^{-16}$ m²/V². Above the characteristic relaxation frequency, the electrostriction strain coefficient drops by 1−2 orders of magnitude to the high-frequency value $|M_{33}^0| \approx 10^{-18}-10^{-17}$ m²/(V²) (Table 1). The frequency relaxation behavior of GdDC ceramic pellets with $x \leq 0.1$ is similar to that reported earlier for 10 mol % GdDC ceramics[21] and for 20 mol % GdDC thin, self-supported membranes.[31]

Well-defined relaxation times are not measurable for ceramic samples with dopant content above 10 mol % Gd (Figure 6d) or 15 mol % Sm (Figure 6b,d) and for small grain, undoped ceria ($x = 0$) ceramics. For these samples, M_{33} varies nonmonotonically with frequency and/or dopant concentration.

3.3. Role of Aliovalent Dopant Concentration in Ceria Electrostriction; Comparisons with Anelasticity and Ionic Conductivity. Two concentration-dependent phenomena are observed for the longitudinal electrostriction strain coefficients: (1) frequency relaxation at concentrations <15 mol % dopant and (2) a 100-fold difference in strain
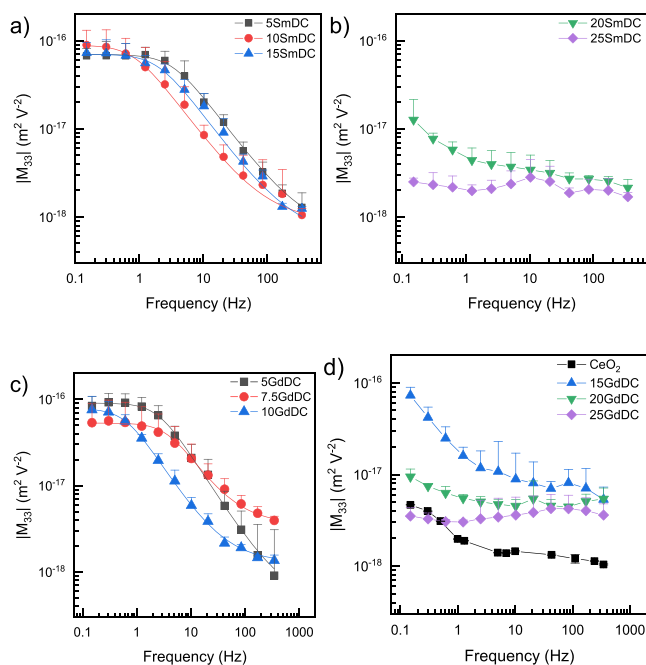
Figure 6. Log−log graphs of the longitudinal electrostriction strain coefficients, $|M_{33}|$, as a function of frequency (f) for the two series: SmDC (a, b) and GdDC (c, d) with various dopant concentrations ≤ 25 mol %. The weak field value of $|M_{33}|$ is used (eq 1). (a, c) $|M_{33}|$ frequency dependence can be described by a Debye-type relaxation curve (solid lines) only for sample pellets containing ≤ 15 mol % Sm or ≤ 10 mol % Gd (Table 1). Error bars include both statistical uncertainty and instrumental accuracy; to increase clarity, only the upper error bar is drawn. Comparison of $|M_{33}|$ for small and large grain 5 mol % Sm-doped ceria ceramics as a function of frequency shows similar behavior as is shown in Figure S3.

magnitude between low- and high-concentration samples. To summarize these data and to remove the possible influence of preparation protocols, we calculated the ratio between the low- and high-frequency electrostriction coefficients as a function of dopant concentration. These values are presented in Figure 7. The nonmonotonic concentration dependence is similar to what was observed during recent anelasticity studies in ceria ceramics[8,9,36] (time-dependent rearrangement of intrinsic strain fields under applied anisotropic stress[37]). Both anelasticity and the unusually large electrostriction strain coefficients have been ascribed to local symmetry breaking in the vicinity of oxygen vacancies.[9,21,34]

Such local symmetry breaking in the fluorite unit cell has recently been explored with reverse Monte Carlo (RMC) simulations of Fourier transformed EXAFS spectra of doped ceria thin films.[34] The initial introduction of randomly distributed lattice defects—aliovalent dopants and charge-compensating oxygen vacancies—causes the Ce−O and Sm−O bond length distributions (mol % Sm ~ 5) to become bimodal; that is, the length distributions display two distinct maxima. An elastic dipole produced in this way can react either to applied mechanical stress, resulting in anelastic behavior, or to an applied electric field, resulting in larger than expected electrostriction (Figures 6 and 7). Because the elastic dipole is relatively massive (comprised of a few atoms), the response is largest at low electric field frequencies. Increased doping, but still within the fluorite phase, extends the bimodality to the Ce−Sm distance distribution. In the current report, we tentatively identify this additional symmetry breaking as the

Table 1. Results of Levenberg−Marquardt Algorithm Fitting [Origin (Microcal); Matlab (Mathworks)] of the Longitudinal Electrostriction Strain Coefficients as a Function of Frequency to the Debye Relaxation Equation (Eq 2) for Ceramic Pellets with ≤15 mol % Sm (i.e., ≤15SmDC) or ≤10 mol % Gd (i.e., ≤10GdDC) Dopant ($R^2 > 0.95$)[a]

	5SmDC	10SmDC	15SmDC	5GdDC	7.5GdDC	10GdDC
$\|M_{33}^0\|$ (10^{-17} m^2/V^2)[b]	7 ± 1	10 ± 3	6 ± 2	9 ± 4	5 ± 1	8 ± 5
$\|M_{33}^\infty\|$ (10^{-17} m^2/V^2)[c]	0.06 ± 0.03	0.03 ± 0.01	0.07 ± 0.05	0.08 ± 0.02	0.27 ± 0.05	0.12 ± 0.05
τ (s)	0.06 ± 0.03	0.06 ± 0.06	0.10 ± 0.06	0.066 ± 0.01	0.032 ± 0.01	0.3 ± 0.2

[a]Frequency range was 0.15−350 Hz. Electric field amplitude ≤0.5 MV/m. Measurements were made in triplicate. [b]Low-frequency, low-field limit. [c]High-frequency longitudinal electrostriction strain coefficients.
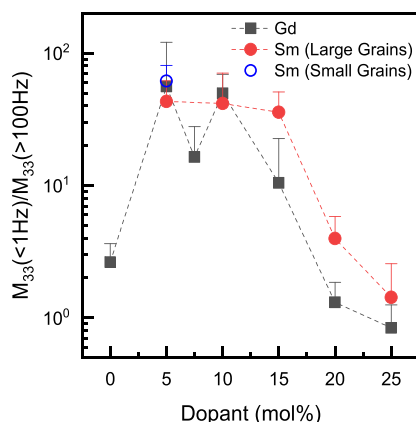
Figure 7. Semilogarithmic plot of the dopant concentration dependence of the ratio of the average longitudinal electrostriction strain coefficients M_{33} at applied electric field frequencies $f < 1$ Hz and $f > 100$ Hz for Gd- or Sm-doped ceria ceramics. Data were obtained as described in the Experimental Section. Error bars are drawn as described in the caption to Figure 6.

structural feature, that limits the amplitude of the electrostrictive strain at higher doping concentrations (Figure 7). We note in addition (Figure S3) that for 5 mol % SmDC ceramics a 35-fold reduction in grain size results in at most ∼30% increase in $|M_{33}|$.

Clearly, the dependence of ceria electrostriction strain coefficients on dopant concentration at room temperature (Figure 7) bears a strong resemblance to that of ceria ionic conductivity at moderately elevated temperatures (300−500 °C). The ionic conductivity increases sharply upon introduction of ∼5 mol % Gd or Sm and gradually decreases at higher doping levels due to a phenomenon often ascribed to the blocking/trapping of oxygen ion diffusion and/or stiffening of the lattice in the vicinity of defect associates.[38] Such a resemblance certainly does not suggest that the origin of giant electrostriction is ionic conductivity; rather, it points to the understanding that both ionic conductivity and electrostriction in ceria originate from lattice defects induced by doping; therefore, both might be expected to display a similarly limited range in which they show an optimum. This correlation, as well as measurement of the dopant concentration dependence of anelastic creep,[9] suggests that there may be an optimal concentration and size of aliovalent dopant that would present an industrially useful combination of ionic conductivity, electrostrictive dimensional change, and minimal frequency relaxation. For example, the largest room temperature electrostriction strain coefficients of ceria have been observed with the dopants (Gd and Sm) and dopant concentrations which, at moderately elevated temperature, also exhibit the highest ionic conductivity. This combination may not be industrially useful because it can lead to chemical degradation

of the electrode material. According to the findings presented in this paper, introducing a higher dopant concentration to reduce ionic conductivity, in combination with a tolerable loss of electromechanical response, may prove to be a possible engineering strategy. We furthermore note that for dense ceria ceramics atomic level organization, that is, intrinsic strain due to lattice defects, appears to be the primary determinant of both the frequency and dopant concentration dependence displayed by the electrostrictive strain, while differences in sample morphology and/or in standard preparation protocols introduce secondary perturbations to the electromechanical behavior.

4. CONCLUSIONS

Optimal engineering design of ceria-based devices requires thorough understanding of their mechanical and electromechanical properties. Here, we have demonstrated that dense ceramic pellets of the well-known ionic conductors $RE_xCe_{1−x}O_{2−x/2}$ ($x ≤ 0.25$, with RE = Gd^{3+} or Sm^{3+}) exhibit electrostrictive strain which exceeds that predicted on the basis of Newnham's classical scaling law by up to 3 orders of magnitude. At frequencies in the range $f = 1−350$ Hz, all samples exhibit longitudinal electrostriction strain coefficients $|M_{33}|$ on the order of $≥10^{-18}$ m^2/V^2. The quasi-static (<1 Hz) longitudinal electrostriction strain coefficients of undoped ceria, as well as doped ceramics with $x > 0.15$ (Sm) or 0.10 (Gd), are comparable. Upon replacing 5 mol % Ce^{4+} with Sm^{3+} or Gd^{3+}, the quasi-static ($f < 1$ Hz) electrostriction coefficient increases by an additional 1−2 orders of magnitude. For SmDC with $x = 0.05−0.15$ and GdDC with $x = 0.05−0.1$, the quasi-static, longitudinal electrostriction coefficient $|M_{33}^0|$ reaches $10^{-17}−10^{-16}$ m^2/V^2, but it exhibits Debye relaxation with a characteristic time τ in the range 60−300 ms. The known anelastic properties of ceria solid solutions have been implicated as the source of this relaxation. On the basis of the similarity of electromechanical behavior of ceria solid solutions as thin films and small or large grain ceramics, we conclude that atomic level organization, that is, intrinsic strain due to lattice defects, is the primary determinant of time and dopant-concentration dependence, while differences in sample morphology and/or standard preparation protocols introduce secondary perturbations to the electrostrictive behavior.

■ ASSOCIATED CONTENT

ⓢ Supporting Information

The Supporting Information is available free of charge at https://pubs.acs.org/doi/10.1021/acsami.0c07799.

> Choice of electrode materials (Figure S1); derivation of electrostriction strain coefficients; anisotropy of the elastic compliance of fluorite single crystals (Figure S2); comparison of electrostrictive coupling of small and large grain Sm-doped ceria ceramics (Figure S3) (PDF)

■ AUTHOR INFORMATION

Corresponding Author

 Igor Lubomirsky − *Department of Materials & Interfaces, Weizmann Institute of Science, Rehovot 76100, Israel;*
 ⊙ orcid.org/0000-0002-2359-2059;
 Email: igor.lubomirsky@weizmann.ac.il

Authors

 Maxim Varenik − *Department of Materials & Interfaces, Weizmann Institute of Science, Rehovot 76100, Israel*

 Juan Claudio Nino − *Department of Materials Science and Engineering, University of Florida, Gainesville, Florida 32611, United States*

 Ellen Wachtel − *Department of Materials & Interfaces, Weizmann Institute of Science, Rehovot 76100, Israel*

 Sangtae Kim − *Department of Materials Science and Engineering, University of California, Davis, Davis, California 95616, United States;* ⊙ orcid.org/0000-0001-6259-5132

 Ori Yeheskel − *Dr. Ori Yeheskel - Consultants, Shoham, Israel*

 Nimrod Yavo − *Department of Materials & Interfaces, Weizmann Institute of Science, Rehovot 76100, Israel*

Complete contact information is available at:
https://pubs.acs.org/10.1021/acsami.0c07799

■ REFERENCES

(1) Mogensen, M.; Sammes, N. M.; Tompsett, G. A. Physical, Chemical and Electrochemical Properties of Pure and Doped Ceria. *Solid State Ionics* **2000**, *129* (1−4), 63−94.

(2) Stefanik, T. S.; Tuller, H. L. Ceria-Based Gas Sensors. *J. Eur. Ceram. Soc.* **2001**, *21* (10−11), 1967−1970.

(3) Schmitt, R.; Spring, J.; Korobko, R.; Rupp, J. L. M. Design of Oxygen Vacancy Configuration for Memristive Systems. *ACS Nano* **2017**, *11* (9), 8881−8891.

(4) Korobko, R.; Kim, S. K.; Kim, S.; Cohen, S. R.; Wachtel, E.; Lubomirsky, I. The Role of Point Defects in the Mechanical Behavior of Doped Ceria Probed by Nanoindentation. *Adv. Funct. Mater.* **2013**, *23* (48), 6076−6081.

(5) Kossoy, A.; Feldman, Y.; Korobko, R.; Wachtel, E.; Lubomirsky, I.; Maier, J. Influence of Point-Defect Reaction Kinetics on the Lattice Parameter of Ce0.8Gd0.2O1.9. *Adv. Funct. Mater.* **2009**, *19* (4), 634−641.

(6) Kossoy, A.; Frenkel, A. I.; Wang, Q.; Wachtel, E.; Lubomirsky, I. Local Structure and Strain-Induced Distortion in CeGd0.2O1.9. *Adv. Mater.* **2010**, *22* (14), 1659−1662.

(7) Greenberg, M.; Wachtel, E.; Lubomirsky, I.; Fleig, J.; Maier, J. Elasticity of Solids with a Large Concentration of Point Defects. *Adv. Funct. Mater.* **2006**, *16* (1), 48−52.

(8) Korobko, R.; Chen, C. T.; Kim, S.; Cohen, S. R.; Wachtel, E.; Yavo, N.; Lubomirsky, I. Influence of Gd Content on the Room Temperature Mechanical Properties of Gd-Doped Ceria. *Scr. Mater.* **2012**, *66* (3−4), 155−158.

(9) Varenik, M.; Cohen, S.; Wachtel, E.; Frenkel, A. I.; Nino, J. C.; Lubomirsky, I. Oxygen Vacancy Ordering and Viscoelastic Mechanical Properties of Doped Ceria Ceramics. *Scr. Mater.* **2019**, *163*, 19−23.

(10) Lloyd, G. J.; McElroy, R. J. On the Anelastic Contribution to Creep. *Acta Metall.* **1974**, *22* (3), 339−348.

(11) Goykhman, N.; Feldman, Y.; Wachtel, E.; Yoffe, A.; Lubomirsky, I. On the Poisson Ratio of Thin Films of Ce0.8Gd0.2O1.9 Ii: Strain-Dependence. *J. Electroceram.* **2014**, *33* (3−4), 180−186.

(12) Kossoy, A.; Wachtel, E.; Lubomirsky, I. On the Poisson Ratio and Xrd Determination of Strain in Thin Films of Ce0.8Gd0.2O1.9. *J. Electroceram.* **2014**, *32* (1), 47−50.

(13) Kraynis, O.; Wachtel, E.; Lubomirsky, I.; Livneh, T. Inelastic Relaxation in Gd-Doped Ceria Films: Micro-Raman Spectroscopy. *Scr. Mater.* **2017**, *137*, 123−126.

(14) Korobko, R.; Lerner, A.; Li, Y. Y.; Wachtel, E.; Frenkel, A. I.; Lubomirsky, I. In-Situ Extended X-Ray Absorption Fine Structure Study of Electrostriction in Gd Doped Ceria. *Appl. Phys. Lett.* **2015**, *106* (4), 042904.

(15) Li, Y. Y.; Kraynis, O.; Kas, J.; Weng, T. C.; Sokaras, D.; Zacharowicz, R.; Lubomirsky, I.; Frenkel, A. I. Geometry of Electromechanically Active Structures in Gadolinium - Doped Cerium Oxides. *AIP Adv.* **2016**, *6* (5), 055320.

(16) Kossoy, A.; Wang, Q.; Korobko, R.; Grover, V.; Feldman, Y.; Wachtel, E.; Tyagi, A. K.; Frenkel, A. I.; Lubomirsky, I. Evolution of the Local Structure at the Phase Transition in CeO2-Gd2O3 Solid Solutions. *Phys. Rev. B: Condens. Matter Mater. Phys.* **2013**, *87* (5), 054101 DOI: 10.1103/PhysRevB.87.054101.

(17) Artini, C.; Costa, G. A.; Pani, M.; Lausi, A.; Plaisier, J. Structural Characterization of the Ceo2/Gd2o3 Mixed System by Synchrotron X-Ray Diffraction. *J. Solid State Chem.* **2012**, *190*, 24−28.

(18) Mishuk, E.; Makagon, E.; Wachtel, E.; Cohen, S. R.; Popovitz-Biro, R.; Lubomirsky, I. Self-Supported Gd-Doped Ceria Films for Electromechanical Actuation: Fabrication and Testing. *Sens. Actuators, A* **2017**, *264*, 333−340.

(19) Hadad, M.; Ashraf, H.; Mohanty, G.; Sandu, C.; Muralt, P. Key-Features in Processing and Microstructure for Achieving Giant Electrostriction in Gadolinium Doped Ceria Thin Films. *Acta Mater.* **2016**, *118*, 1−7.

(20) Korobko, R.; Patlolla, A.; Kossoy, A.; Wachtel, E.; Tuller, H. L.; Frenkel, A. I.; Lubomirsky, I. Giant Electrostriction in Gd-Doped Ceria. *Adv. Mater.* **2012**, *24* (43), 5857−5861.

(21) Yavo, N.; Yeheskel, O.; Wachtel, E.; Ehre, D.; Frenkel, A. I.; Lubomirsky, I. Relaxation and Saturation of Electrostriction in 10 Mol % Gd-Doped Ceria Ceramics. *Acta Mater.* **2018**, *144*, 411−418.

(22) Yavo, N.; Smith, A. D.; Yeheskel, O.; Cohen, S. R.; Korobko, R.; Wachtel, E.; Slater, P. R.; Lubomirsky, I. Large Nonclassical Electrostriction in (Y, Nb)-Stabilized Delta-Bi2O3. *Adv. Funct. Mater.* **2016**, *26* (7), 1138−1142.

(23) Li, Q.; Lu, T.; Schiemer, J.; Laanait, N.; Balke, N.; Zhang, Z.; Ren, Y.; Carpenter, M. A.; Wen, H. D.; Li, J. Y.; Kalinin, S. V.; Liu, Y. Giant Thermally-Enhanced Electrostriction and Polar Surface Phase in La2Mo2O9 Oxygen Ion Conductors. *Phys. Rev. Mater.* **2018**, *2* (4), 041403.

(24) Kabir, A.; Santucci, S.; Van Nong, N.; Varenik, M.; Lubomirsky, I.; Nigon, R.; Muralt, P.; Esposito, V. Effect of Oxygen Defects Blocking Barriers on Gadolinium Doped Ceria (GDC) Electro-Chemo-Mechanical Properties. *Acta Mater.* **2019**, *174*, 53−60.

(25) Kabir, A.; Kyu Han, J.; Merle, B.; Esposito, V. The Role of Oxygen Defects on the Electro-Chemo-Mechanical Properties of Highly Defective Gadolinium Doped Ceria. *Mater. Lett.* **2020**, *266*, 127490.

(26) Li, L. P.; Nino, J. C. Ionic Conductivity across the Disorder-Order Phase Transition in the SmO1.5-CeO2 System. *J. Eur. Ceram. Soc.* **2012**, *32* (13), 3543−3550.

(27) Li, L. P.; Kasse, R.; Phadke, S.; Qiu, W.; Huq, A.; Nino, J. C. Ionic Conductivity across the Disorder-Order Phase Transition in the NdO1.5-CeO2 System. *Solid State Ionics* **2012**, *221*, 15−21.

(28) Yavo, N.; Nissenbaum, A.; Wachtel, E.; Shaul, T. E.; Mendelson, O.; Kimmel, G.; Kim, S.; Lubomirsky, I.; Yeheskel, O. Rapid Sintering Protocol Produces Dense Ceria-Based Ceramics. *J. Am. Ceram. Soc.* **2018**, *101* (11), 4968−4975.

(29) Mendelson, M. I. Average Grain Size in Polycrystalline Ceramics. *J. Am. Ceram. Soc.* **1969**, *52* (8), 443−446.

(30) Mishuk, E.; Ushakov, A.; Makagon, E.; Cohen, S. R.; Wachtel, E.; Paul, T.; Tsur, Y.; Shur, V. Y.; Kholkin, A.; Lubomirsky, I. Electro-Chemomechanical Contribution to Mechanical Actuation in Gd-Doped Ceria Membranes. *Adv. Mater. Interfaces* **2019**, *6* (6), 1801592.

(31) Ushakov, A. D.; Mishuk, E.; Alikin, D. O.; Slautin, B. N.; Esin, A. A.; Baturin, I. S.; Shur, V. Y.; Lubomirsky, I.; Kholkin, A. L. Thermal Excitation Contribution into the Electromechanical Performance of Self-Supported Gd-Doped Ceria Membranes. *IOP Conf. Ser.: Mater. Sci. Eng.* **2017**, *256*, 012008.

(32) Newnham, R. E.; Sundar, V.; Yimnirun, R.; Su, J.; Zhang, Q. M. Electrostriction: Nonlinear Electromechanical Coupling in Solid Dielectrics. *J. Phys. Chem. B* **1997**, *101* (48), 10141−10150.

(33) Newnham, R. E. *Properties of Materials: Anisotropy, Symmetry, Structure*; Oxford University Press: Oxford, 2005; p xii, 378 pp.

(34) Kraynis, O.; Timoshenko, J.; Huang, J.; Singh, H.; Wachtel, E.; Frenkel, A. I.; Lubomirsky, I. Modeling Strain Distribution at the Atomic Level in Doped Ceria Films with Extended X-Ray Absorption Fine Structure Spectroscopy. *Inorg. Chem.* **2019**, *58*, 7527.

(35) Marrocchelli, D.; Bishop, S. R.; Tuller, H. L.; Yildiz, B. Understanding Chemical Expansion in Non-Stoichiometric Oxides: Ceria and Zirconia Case Studies. *Adv. Funct. Mater.* **2012**, *22* (9), 1958−1965.

(36) Yavo, N.; Noiman, D.; Wachtel, E.; Kim, S.; Feldman, Y.; Lubomirsky, I.; Yeheskel, O. Elastic Moduli of Pure and Gadolinium Doped Ceria Revisited: Sound Velocity Measurements. *Scr. Mater.* **2016**, *123*, 86−89.

(37) Nowick, A. S.; Berry, B. S. *Anelastic Relaxation in Crystalline Solids*; Academic Press: New York, 1972; p xv, 677 pp.

(38) Koettgen, J.; Grieshammer, S.; Hein, P.; Grope, B. O. H.; Nakayama, M.; Martin, M. Understanding the Ionic Conductivity Maximum in Doped Ceria: Trapping and Blocking. *Phys. Chem. Chem. Phys.* **2018**, *20* (21), 14291−14321.